

## Article

# Role of Mixed Oxides in Hydrogen Production through the Dry Reforming of Methane over Nickel Catalysts Supported on Modified $\gamma$ -Al<sub>2</sub>O<sub>3</sub>

Ahmed Sadeq Al-Fatesh <sup>1,\*</sup>, Mayankkumar Lakshmanbhai Chaudhary <sup>2</sup>, Anis Hamza Fakeeha <sup>1,3</sup>,  
Ahmed Aidid Ibrahim <sup>1</sup>, Fahad Al-Mubaddel <sup>1,3</sup>, Samsudeen Olajide Kasim <sup>1</sup>,  
Yousef Abdulrahman Albaqmaa <sup>1</sup>, Abdulaziz A. Bagabas <sup>4</sup>, Rutu Patel <sup>2</sup> and Rawesh Kumar <sup>2</sup>

- <sup>1</sup> Chemical Engineering Department, College of Engineering, King Saud University, P.O. Box 800, Riyadh 11421, Saudi Arabia; anishf@ksu.edu.sa (A.H.F.); aididwthts2011@gmail.com (A.A.I.); falmubaddel@ksu.edu.sa (F.A.-M.); sofkolajide2@gmail.com (S.O.K.); youssef201629@gmail.com (Y.A.A.)
- <sup>2</sup> Sankalchand Patel University, Visnagar 384315, India; mayankchaudhary8326@gmail.com (M.L.C.); rutupatel1145@gmail.com (R.P.); kr.rawesh@gmail.com (R.K.)
- <sup>3</sup> King Abdullah City for Atomic & Renewable Energy, Energy Research & Innovation Center (ERIC) in Riyadh, Riyadh 11451, Saudi Arabia
- <sup>4</sup> National Petrochemical Technology Center (NPTC), Materials Science Research Institute (MSRI), King Abdulaziz City for Science and Technology (KACST), P.O. Box 6086, Riyadh 11442, Saudi Arabia; abagabas@hotmail.com
- \* Correspondence: aalfatesh@ksu.edu.sa; Tel.: +966-11-467-6859



**Citation:** Al-Fatesh, A.S.; Chaudhary, M.L.; Fakeeha, A.H.; Ibrahim, A.A.; Al-Mubaddel, F.; Kasim, S.O.; Albaqmaa, Y.A.; Bagabas, A.A.; Patel, R.; Kumar, R. Role of Mixed Oxides in Hydrogen Production through the Dry Reforming of Methane over Nickel Catalysts Supported on Modified  $\gamma$ -Al<sub>2</sub>O<sub>3</sub>. *Processes* **2021**, *9*, 157. <https://doi.org/10.3390/pr9010157>

Received: 15 December 2020

Accepted: 8 January 2021

Published: 15 January 2021

**Publisher's Note:** MDPI stays neutral with regard to jurisdictional claims in published maps and institutional affiliations.



**Copyright:** © 2021 by the authors. Licensee MDPI, Basel, Switzerland. This article is an open access article distributed under the terms and conditions of the Creative Commons Attribution (CC BY) license (<https://creativecommons.org/licenses/by/4.0/>).

**Abstract:** H<sub>2</sub> production through dry reforming of methane (DRM) is a hot topic amidst growing environmental and atom-economy concerns. Loading Ni-based reducible mixed oxide systems onto a thermally stable support is a reliable approach for obtaining catalysts of good dispersion and high stability. Herein, NiO was dispersed over MO<sub>x</sub>-modified- $\gamma$ -Al<sub>2</sub>O<sub>3</sub> (M = Ti, Mo, Si, or W; x = 2 or 3) through incipient wetness impregnation followed by calcination. The obtained catalyst systems were characterized by infrared, ultraviolet–visible, and X-ray photoelectron spectroscopies, and H<sub>2</sub> temperature-programmed reduction. The mentioned synthetic procedure afforded the proper nucleation of different NiO-containing mixed oxides and/or interacting-NiO species. With different modifiers, the interaction of NiO with the  $\gamma$ -Al<sub>2</sub>O<sub>3</sub> support was found to change, the Ni<sup>2+</sup> environment was reformed exclusively, and the tendency of NiO species to undergo reduction was modified greatly. Catalyst systems 5Ni3MAI (M = Si, W) comprised a variety of species, whereby NiO interacted with the modifier and the support (e.g., NiSiO<sub>3</sub>, NiAl<sub>2</sub>O<sub>4</sub>, and NiWO<sub>3</sub>). These two catalyst systems displayed equal efficiency, >70% H<sub>2</sub> yield at 800 °C, and were thermally stable for up to 420 min on stream. 5Ni3SiAl catalyst regained nearly all its activity during regeneration for up to two cycles.

**Keywords:** H<sub>2</sub> production; mixed oxide; NiAl<sub>2</sub>O<sub>4</sub>; NiWO<sub>3</sub>; NiSiO<sub>3</sub>; NiO-interacting species

## 1. Introduction

Hydrogen (H<sub>2</sub>) is a green energy source. In fact, the energy content of this molecule is three times higher than that of gasoline [1]. H<sub>2</sub> is a critical feedstock for the chemical industry in oil refining, fertilizer production, and fuel cell manufacture [2]. Notably, biomass pyrolysis and biomass gasification have always been environmentally questionable approaches to hydrogen production; moreover, the implementation of these methods renders H<sub>2</sub> isolation and purification quite difficult, as the desired product associates with many side-products [3]. A more convenient approach is hydrogen production from compounds such as ethanol [4], glycerol [5], glucose [6], starch, and catechol [7], by steam or thermal reforming over a heterogeneous catalyst. Environmental concerns and the high demand for atom-economies have driven the development of hydrogen production methods, relying

on clean sources, such as water splitting, thermal reforming of methane, steam reforming of methane, and CO<sub>2</sub> (dry) reforming of methane (DRM) [8,9]. DRM in particular, has drawn great deal of attention globally because it fulfils the goal of hydrogen production while raising hope for the reduction of the atmospheric concentrations of carbon dioxide and methane, the two gases whose emissions are most responsible for global warming.

From a catalytic standpoint, metal oxide and mixed metal oxide systems have attracted the attention of the industry, due to their ease of formation, development of mixed oxide potential, tuneable surface topology, high temperature sustainability, and ease of handling in drastic industrial conditions [10]. Ni-based catalysts supported on thermally-stable neutral SiO<sub>2</sub> [11], acidic Al<sub>2</sub>O<sub>3</sub> [12], and reducible TiO<sub>2</sub> [13,14] have been investigated thoroughly in recent years. Due to the need of acid-base bi-functional catalyst for DRM, TiO<sub>2</sub> and Al<sub>2</sub>O<sub>3</sub> supports were investigated more than SiO<sub>2</sub>. Reducibility characteristics of TiO<sub>2</sub> controls the coke deposition. However, the coverage of Ni species by the TiO<sub>x</sub> and partial transformation of amorphous titania phase into the anatase phase limit its DRM application [15]. Nevertheless, the addition of 25% Al<sub>2</sub>O<sub>3</sub> to TiO<sub>2</sub> support was found to be beneficial [16]. Overall, the highly thermal stability, low cost, wide availability, and strong metal–support interaction favor alumina as the support for Ni dispersion [17]. Nickel form bulk NiO is sintered into large Ni particles during DRM, and these nanoparticles are encapsulated by carbon. Due to encapsulation and loss of catalytic active sites, the catalytic activity was affected badly [18]. Alumina supported Nickel catalyst system has mixed oxide NiAl<sub>2</sub>O<sub>4</sub> phases, confirming strong metal–support interaction in the catalyst system. Reduced Ni derived from NiAl<sub>2</sub>O<sub>4</sub> favors the formation of carbon filament by putting the Ni particle on tip. Therefore, it showed high resistant to sintering and coking without affecting the catalytic activity. Al<sub>2</sub>O<sub>3</sub> nanosheet provides superior anchoring surface (100) for Ni nanoparticle and so Ni-based catalysts supported on nanosheet (S) were claimed to result in more than 85% CO<sub>2</sub> and CH<sub>4</sub> conversion with excellent H<sub>2</sub> and CO selectivity [19]. However, Ni-based catalysts supported on nanofiber exhibited superior catalytic stability due to its abundant confined spaces and steady chemisorption behavior. Under other synthetic methodology, such as evaporation-induced self-assembly method [20] and microwave-assisted combustion [21] and atomic layer deposition [22] method have drawn attentions. As a sandwiched catalyst Al<sub>2</sub>O<sub>3</sub>/Ni/Al<sub>2</sub>O<sub>3</sub> (prepared by atomic layer deposition) prevented Ni gathering over alumina by coating of porous Al<sub>2</sub>O<sub>3</sub> thin-film over Ni/Al<sub>2</sub>O<sub>3</sub>. Moreover, Ni had double interaction with Al<sub>2</sub>O<sub>3</sub> in this catalyst system and so it was claimed nearly 100% CO<sub>2</sub> and CH<sub>4</sub> conversion with absolute selectivity towards CO and H<sub>2</sub>.

Incorporation of Cu, Mo, Si, Sr, B, Ca, Mg, Ba, Ga, Gd, Zn, Ti, W, Mn, Co, Zr, Ce, La, and Yb, in the alumina supported Ni catalyst was examined in the search of high catalytic activity and coke resistance. The addition of Cu resulted in inferior performance due to sintering of Cu particles and presence of free NiO (weak metal support interaction) [23,24]. The inferior performance of Mo promoted Ni/Al<sub>2</sub>O<sub>3</sub> catalyst was due to weak metal support interaction, the formation of MoNi<sub>4</sub> phase and the lower basicity of catalyst [25]. Modification of Ni/Al<sub>2</sub>O<sub>3</sub> with 11.9 wt% W modified Ni/Al<sub>2</sub>O<sub>3</sub> showed 76% less carbon decomposition than unmodified samples [26]. It was supposed that Ni-W alloy formed during reduction and hindered the carbon deposition inside the lattice and further tungsten carbide formed and carried out carbon gasification. However, Ni.W alloy formation caused inferior catalytic activity because alloy might be less active for methane decomposition. Monolithic Ni-Al<sub>2</sub>O<sub>3</sub>-SiC catalyst was claimed higher CO<sub>2</sub> conversion (>40%) and CH<sub>4</sub> conversion (~30%) than Ni/Al<sub>2</sub>O<sub>3</sub> catalyst due to stereo-structure and highly dispersed Ni species [27]. The addition of 0.75 wt% Sr addition improved the metal (Ni) support (Al<sub>2</sub>O<sub>3</sub>) interaction and boosts Lewis basicity. It favored CO<sub>2</sub> absorption and dissociation which in turn decreased the coke deposition [28]. Modification of 0.6–5.6 wt% B<sub>2</sub>O<sub>3</sub> led to size-reduction of Ni particles which induced 74–86% less coke formation during DRM without significantly affecting activity and selectivity [29]. Among the basic modifier: MgO, CaO and BaO; it was found that 3 wt% MgO addition improved the catalytic activity (>70%



and by H<sub>2</sub> temperature-programmed reduction (H<sub>2</sub>-TPR). We also report the results of tests run on these systems for H<sub>2</sub> production. We attempted to identify the metal, metal oxides, and mixed metal oxides responsible for H<sub>2</sub> production through DRM. Crucially, this information would be useful in the design of metal oxide matrix catalyst systems suitable for the industrial production of H<sub>2</sub> through DRM.

## 2. Results

### 2.1. Catalytic Activity

Data reflecting the catalytic activity of the prepared catalysts, in terms of H<sub>2</sub> yield over 420 min on stream at 700 °C are reported in Figure 2A. On the other hand, Figure 2B shows values for the H<sub>2</sub> yield at different reaction temperatures. Among the investigated catalysts, 5Ni<sub>3</sub>SiAl and 5Ni<sub>3</sub>WAl exhibited the highest catalytic performance, and the activities and stabilities of these two species were found to be identical. The H<sub>2</sub> yield recorded for both catalysts over 420 min on stream was about 62% at 700 °C. The H<sub>2</sub> yield over 5Ni<sub>3</sub>MoAl catalyst was 47% after 20 min on stream, which decreased to 39% after 420 min on stream. The catalytic performance of 5Ni<sub>3</sub>TiAl was found to be the worst: ~30% H<sub>2</sub> yield after 420 min on stream. Notably, the H<sub>2</sub> yield in the presence of all catalyst systems increased as the reaction temperature increased. At 800 °C, the use of 5Ni<sub>3</sub>SiAl and 5Ni<sub>3</sub>WAl was associated with more than 70% H<sub>2</sub> yield, whereas in the case of 5Ni<sub>3</sub>MoAl and 5Ni<sub>3</sub>TiAl, H<sub>2</sub> yield was measured to be around 60%. Higher conversion trend at higher temperature indicated the endothermic nature of DRM reaction. For silicon- or tungsten-modified alumina-supported nickel catalyst system, the rise of H<sub>2</sub> yield with temperature were similar. For titanium- and molybdenum-modified catalyst systems, the rise of H<sub>2</sub> yield with temperature were similar up to 650 °C, and after this temperature, molybdenum-modified catalyst system showed better H<sub>2</sub> yield.

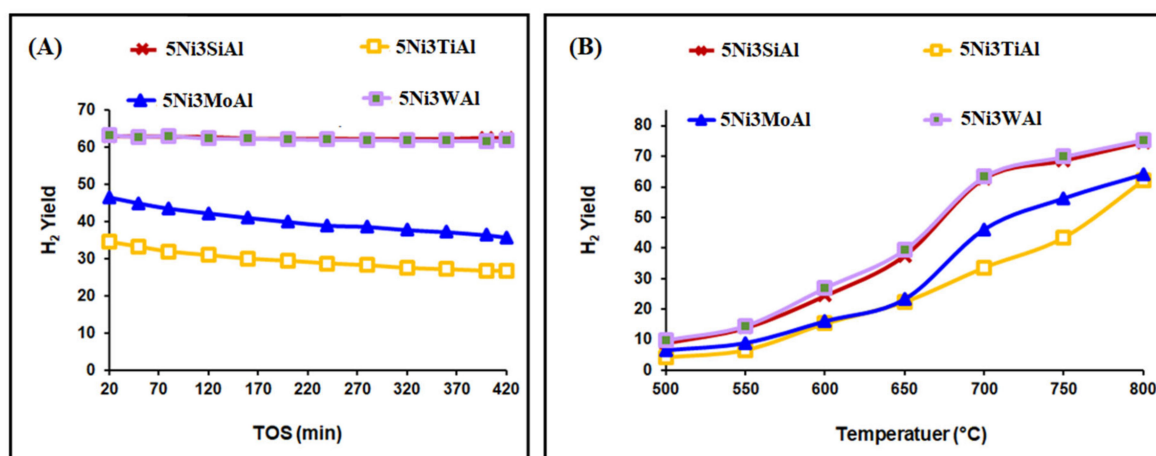


**Figure 2.** (A) H<sub>2</sub> yield over different catalyst systems up to 420 min TOS at 700 °C; (B) H<sub>2</sub> yield over different catalyst systems in the 500–800 °C reaction temperature range.

### 2.2. Result

SEM images and EDX patterns of 5Ni<sub>3</sub>MAI (M = W, Si, Mo, Ti) are shown in Figures S1 and S2, respectively. EDX patterns showed the presence of all claimed elements in the catalyst systems (Figure S2). In all IR spectra, the sharp peak at 1644 cm<sup>-1</sup> and the broad intense peak at 3450 cm<sup>-1</sup> could be due to the bending and stretching vibrations, respectively, of adsorbed water molecules or surface hydroxyl groups [40]. The IR peaks in the 600–750 cm<sup>-1</sup> wavenumber range could be attributed to the vibrations of AlO<sub>6</sub> octahedral units (Al-O bonds in an octahedral environment), whereas those in the 750–850 cm<sup>-1</sup> range could be attributed to AlO<sub>4</sub> tetrahedral units (Al-O bonds in a tetrahedral environment) [41]. The three peaks in the 1640–1350 cm<sup>-1</sup> wavenumber range

might be assigned to the bending vibration of the water molecules coordinated to different unsaturated surface sites. Furthermore, the peak at  $1635\text{ cm}^{-1}$  could be due to the vibration of physically adsorbed water molecules, whereas the peak at  $1380\text{ cm}^{-1}$  could be due to the bending vibration of water molecules coordinating tetrahedral aluminum [40]. The IR spectrum of  $\gamma\text{-Al}_2\text{O}_3$  was characterized by the presence of three peaks at  $1635\text{ cm}^{-1}$ ,  $1517\text{ cm}^{-1}$ , and  $1382\text{ cm}^{-1}$  [42]. IR peaks in the  $400\text{--}470\text{ cm}^{-1}$  wavenumber range could be due to the vibration of the Ni-O bond [43] in free NiO or to the said bond in mixed oxides such as  $\text{NiSiO}_4$ ,  $\text{NiAl}_2\text{O}_4$ ,  $\text{NiTiO}_3$ ,  $\text{NiWO}_4$ , and  $\text{NiMoO}_4$ . The IR spectrum of the titanium-modified catalyst sample,  $5\text{Ni}_3\text{TiAl}$ , (Figure 3A,B and Figure S3A,B), comprised an absorption peak at  $433\text{ cm}^{-1}$ , which could be due to the Ni-O vibration of free NiO species in a cubic lattice, and peaks at  $455\text{ cm}^{-1}$  and  $547\text{ cm}^{-1}$ , which may be due to the Ni-O bond vibration of  $\text{NiTiO}_3$  [44,45]. After NiO loading, the peak due to  $\text{TiO}_2$  in the low-frequency region of the spectrum (below  $500\text{ cm}^{-1}$ ) was replaced by peaks due to Ni-O vibrations, which was an indication of the extent of interaction of NiO species with the modifier over the support.

The IR spectrum of the molybdenum-containing catalyst,  $5\text{Ni}_3\text{MoAl}$ , (Figure 3C,D and Figure S3A,B), comprised a band at  $424\text{ cm}^{-1}$  due to Ni-O bond vibration, which appeared at lower wavenumber values than that attributed to free NiO ( $433\text{ cm}^{-1}$ ) in the spectrum of the titanium-modified catalyst. No other prominent peaks due to Ni-O vibrations were noticed in the spectrum of the molybdenum-containing catalyst, indicating the deformation of cubic NiO species and the formation of species, whereby NiO interacted with the support, the modifier, or both [46,47]. After NiO loading, the peak due to  $\text{MoO}_x$  in the low-frequency region was completely replaced by the vibrational peak of Ni-O, indicating the extent of the interaction of NiO species with the modifier over the support.

In the IR spectrum of  $5\text{Ni}_3\text{SiAl}$  (Figure 3E,F and Figure S3A,B), Ni-O vibrational peaks at  $430\text{ cm}^{-1}$ , due to free NiO, and  $403\text{ cm}^{-1}$ , due to strongly interacting-NiO (as a result of the weakening of the Ni-O bond), were noticed, alongside a peak at  $453\text{ cm}^{-1}$ , due to the Si-O-Si bending vibration [48], and one at  $481\text{ cm}^{-1}$ , due to the asymmetric vibration of Si-O [49]. However, the S-O asymmetric vibration peak was not noticed in the spectrum of  $\text{SiO}_2\text{-Al}_2\text{O}_3$ , indicating that this vibration was related to an interaction of NiO with silica species or to the presence of amorphous nickel silicate species. This finding is in agreement with our previous claim of an interaction of NiO species, as deduced from  $\text{H}_2$ -TPR data, and the absence of nickel silicate phases, as deduced from X-ray diffraction data. The IR peak and its shoulder appearing in the  $549\text{--}560\text{ cm}^{-1}$  wavenumber range could be attributed to the presence of Al-O-Ni bonding interactions in  $\text{NiAl}_2\text{O}_4$  [50].

In both  $5\text{Ni}_3\text{SiAl}$  and  $5\text{Ni}_3\text{WAl}$ , following NiO loading, the infrared spectra of the modified catalysts became populated with intense peaks, indicating the presence and dispersion of a wide variety of species, whereby NiO interacted with catalyst components on the catalyst surface. In the IR spectrum of  $5\text{NiWAl}$  (Figure 3G,H) the low-intensity absorption bands below  $500\text{ cm}^{-1}$  could be attributed to the stretching vibrations of  $\text{NiO}_6$  polyhedral in  $\text{NiWO}_4$  species [51].

The infrared spectra of the catalyst samples showed a clear shift of Ni-O peak from  $433\text{ cm}^{-1}$  (for  $5\text{Ni}_3\text{TiAl}$ ) to  $424\text{ cm}^{-1}$  (for  $5\text{Ni}_3\text{MoAl}$ ) and  $403\text{ cm}^{-1}$  (for  $5\text{Ni}_3\text{SiAl}$ ). That reflects the presence of "free NiO" species in  $5\text{Ni}_3\text{TiAl}$ ; NiO species interacted with the modifier in  $5\text{Ni}_3\text{MoAl}$  and NiO species strongly interacted with the support/modifier in  $5\text{Ni}_3\text{SiAl}$ .  $5\text{Ni}_3\text{WAl}$  catalyst samples had a wide interaction NiO species as it showed stretching vibration of  $\text{NiO}_6$  polyhedral.

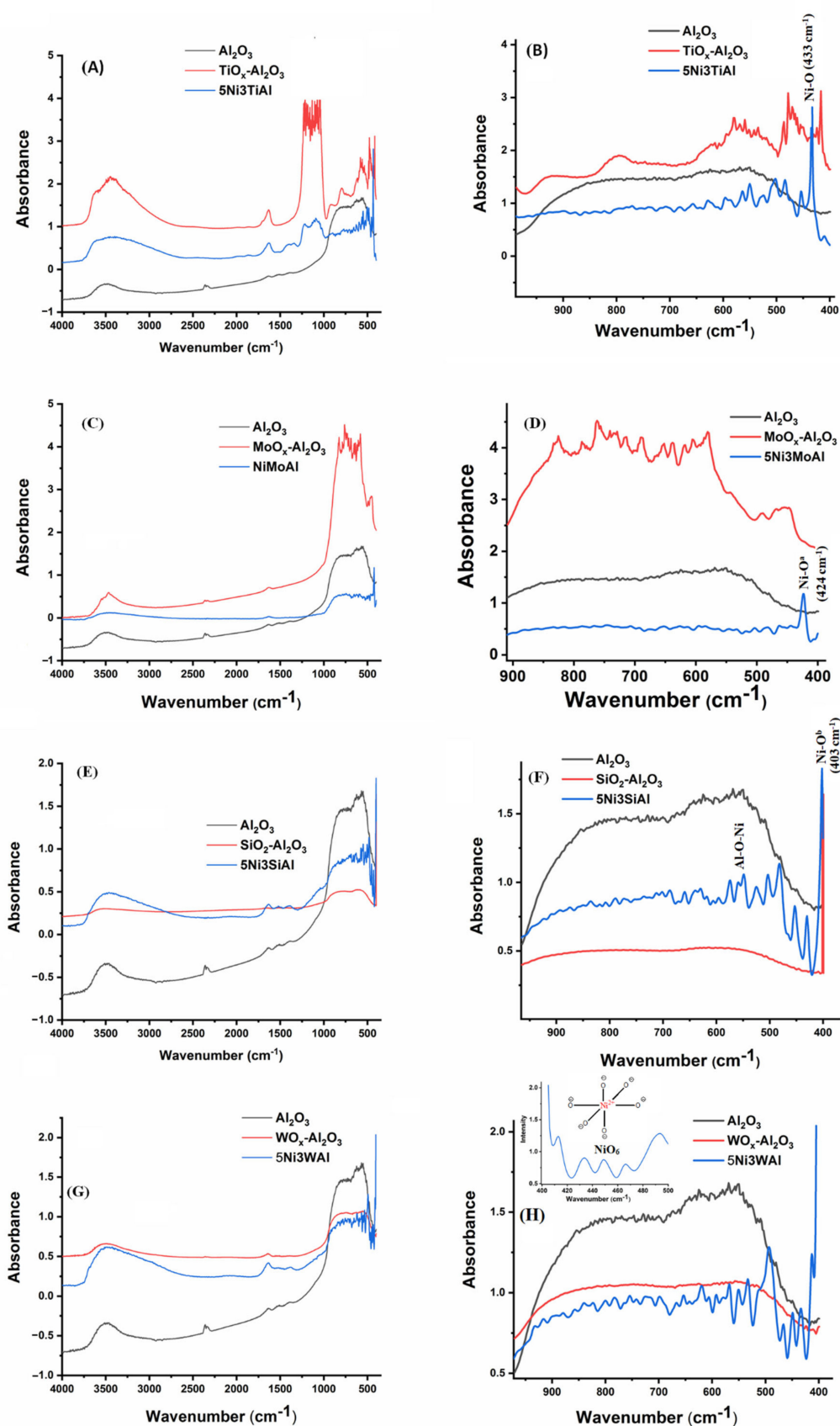


**Figure 3.** (A–H) Infrared spectra of different catalyst systems. In (D), Ni-O<sup>a</sup> indicates NiO species that interacted with the support. In (F) Ni-O<sup>b</sup> indicates NiO species that strongly interacted with the support. In (H) inset indicates stretching vibration peaks of NiO<sub>6</sub> polyhedra in NiWO<sub>4</sub> species.

UV–Vis spectroscopy is the most suitable characterization technique to understand the electronic environment of  $\text{Ni}^{2+}$  or  $d^8$ -configuration systems. The UV–Vis absorption spectra of all catalyst samples are reported in Figure 4. The peak observed at 250–350 nm is associated with the charge transfer transition from  $\text{O}^{2-}$  to  $\text{Ni}^{2+}$  in an octahedral coordination environment ( $\text{O}^{2-} \rightarrow \text{Ni}^{2+}$ ) in the NiO lattice [29]. The peak centered at around 410 nm is associated with the d-d transition from the  ${}^3A_{2g}(\text{F})$  state to the  ${}^3T_{1g}(\text{P})$  state of  $\text{Ni}^{2+}$  in an octahedral environment, whereas the doublet peak with maxima at 593 nm and 634 nm were attributed to the d-d transition from the  ${}^3T_1(\text{F})$  state to the  ${}^3T_1(\text{P})$  state of  $\text{Ni}^{2+}$  in a tetrahedral environment [52]. Among all four catalysts, only the silicon- and tungsten-containing catalysts (5Ni3SiAl and 5Ni3WAl) included  $\text{Ni}^{2+}$  ions in both tetrahedral and octahedral environments. The  $\text{NiAl}_2\text{O}_4$  phase is known to comprise  $\text{Ni}^{2+}$  ions in both tetrahedral and octahedral coordination environments. Therefore, 5Ni3SiAl and 5Ni3WAl may contain  $\text{NiAl}_2\text{O}_4$  phases. In the case of the other catalysts, the mentioned bands either displayed low intensity or had shifted toward higher wavelengths, indicating a weak interaction between the modifier and  $\text{Ni}^{2+}$  and the support. In the case of the titanium-containing catalyst (5Ni3TiAl), no peaks attributable to  $\text{Ni}^{2+}$  ions in tetrahedral environments were observed, indicating the absence of an  $\text{NiAl}_2\text{O}_4$  phase. By contrast, the UV–Vis spectrum of 5Ni3TiAl displayed a peak at 740 nm attributable to  $\text{Ni}^{2+}$  in an octahedral coordination environment, as segregated or crystallized NiO which was as near as bulk NiO [53], indicating that octahedral coordinated  $\text{Ni}^{2+}$  was present in segregated form in 5Ni3TiAl. An additional hump in the 260–330 nm wavelength range for 5Ni3TiAl could be assigned to a charge transfer from  $\text{O}^{2-}$  to octahedral/tetrahedral  $\text{Ti}^{4+}$  ( $\text{O}^{2-} \rightarrow \text{Ti}^{4+}$ ) in a possible  $\text{NiTiO}_3$  phase [44]. The hump in the 280–330 nm wavelength range observed in the UV–Vis spectrum of 5Ni3MoAl could be attributed to a charge transfer from  $\text{O}^{2-}$  to octahedral/tetrahedral  $\text{Mo}^{6+}$  ( $\text{O}^{2-} \rightarrow \text{Mo}^{6+}$ ) in a possible  $\text{NiMoO}_4$  phase/ $\text{Al}_2(\text{MoO}_4)_3$  phase [54].

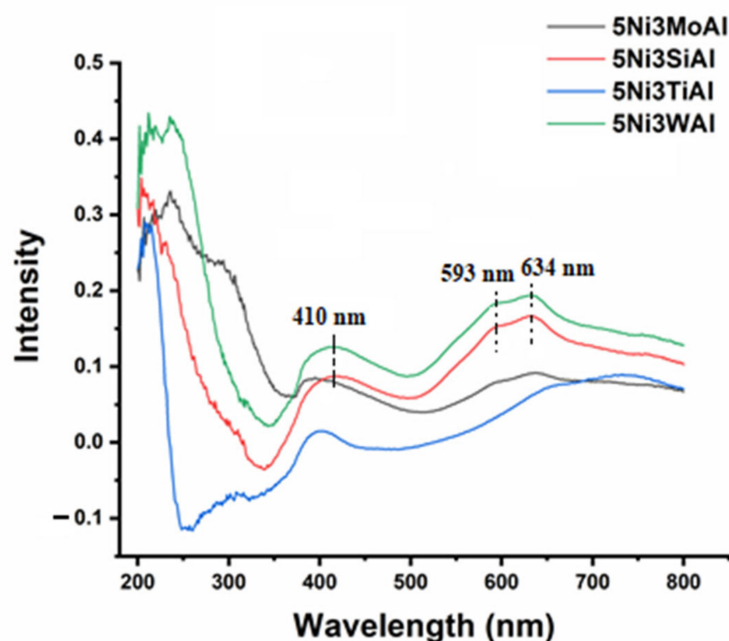


**Figure 4.** Ultraviolet–visible spectra of different catalyst systems. Peak at 410 nm is associated with d–d transition  ${}^3A_{2g}(\text{F}) \rightarrow {}^3T_{1g}(\text{P})$  in  $\text{Ni}^{2+}$  in an octahedral environment. Peaks at 593 and 634 nm are associated with the d–d transition  ${}^3T_1(\text{F}) \rightarrow {}^3T_1(\text{P})$  in  $\text{Ni}^{2+}$  in a tetrahedral environment.

In order to clarify further the interaction of Ti and Mo with the support and with catalytic active sites (NiO), Al (2p, 2s) XPS analysis was conducted on 5Ni3TiAl and 5Ni3MoAl (Figure 5A). The Al (2p) XPS spectrum of 5Ni3TiAl was characterized by peaks

at 74.30 eV and at 119.17 eV. These peaks were quite similar to those observed in the Al (2p) XPS spectrum of pure  $\gamma$ -Al<sub>2</sub>O<sub>3</sub> [55]. This evidence indicated that the  $\gamma$ -Al<sub>2</sub>O<sub>3</sub> support doesn't interact with TiO<sub>2</sub> and NiO. However, in the presence of molybdenum as a modifier, a substantial shift to lower energy values (to 71.5 eV and 116.34 eV) was observed for the mentioned peaks in the Al (2p) spectra. This shift was indicative of changes in the electronic environment around Al ions, resulting from an increase in negative charge in the vicinity of Al<sup>3+</sup> due to an excess of oxygen atoms around it. It may indicate an oxide enrichment resulting from the formation of Al<sub>2</sub>(MoO<sub>4</sub>)<sub>3</sub> [56]. However, the absence of peak shifts to higher energy in the case of the Al (2p) and Al (2s) XPS spectra of 5Ni3MoAl indicates a poor interaction between NiO and the  $\gamma$ -Al<sub>2</sub>O<sub>3</sub> support (i.e., the formation of a NiAl<sub>2</sub>O<sub>4</sub> phase was not observed) [57,58]. Notably, Mo (3d) XPS analysis was also carried out on 5Ni3MoAl (Figure 5B). The Mo (3d) XPS spectrum of this catalyst showed a doublet peak with maxima at 234.75 eV and 235.8 eV, which is attributable to the interaction of NiO with MoO<sub>x</sub> species [59,60], and a peak at 233.52 eV, which is attributable to a strong interaction between MoO<sub>3</sub> and  $\gamma$ -Al<sub>2</sub>O<sub>3</sub> or the formation of Al<sub>2</sub>(MoO<sub>4</sub>)<sub>3</sub> [61]. Overall, 5Ni3TiAl can be said to comprise negligibly interacting species, whereas 5Ni3MoAl may include species whereby NiO interacted with MoO<sub>x</sub>, and MoO<sub>3</sub> interacted with  $\gamma$ -Al<sub>2</sub>O<sub>3</sub>, although little interaction appeared to exist between NiO and the  $\gamma$ -Al<sub>2</sub>O<sub>3</sub> support [62].

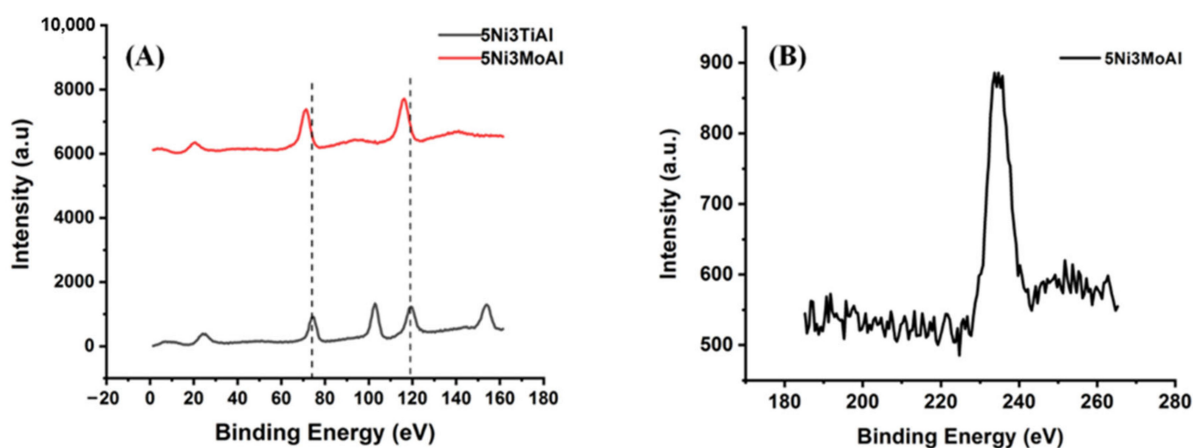


**Figure 5.** (A) Al (2p, 2s) X-ray photoelectron spectra of catalysts 5Ni3TiAl and 5Ni3MoAl and (B) Mo (3d) X-ray photoelectron spectrum of 5Ni3MoAl.

Till now, catalysts 5Ni3SiAl and 5Ni3WAl were thus found to be enriched with NiO species interacting with the support and the modifier. The tendency of these species to undergo reduction needs, however, to be determined because only reduced nickel species (i.e., metallic nickel) can initiate CH<sub>4</sub> decomposition for hydrogen production through DRM [63,64]. In order to determine their reducibility, H<sub>2</sub>-TPR experiments were carried out for 5Ni3SiAl and 5Ni3WAl catalysts (Figure 6). The deconvoluted peak profiles are shown in Figure S4. These reduction peaks can be categorized into four regions; region I 200–400 °C, region II 400–700 °C, region III 700–900 °C, and region IV 900–1000 °C [65]. The H<sub>2</sub>-TPR profile of 5Ni3SiAl was characterized by a low prominent reduction peak in region I and largely overlapped peaks in regions II and III. The less prominent peak in region I was due to reduction of free NiO species. Region II showed reduction peak for NiO interacting with the modifier or NiSiO<sub>3</sub>, whereas region III showed reduction peaks for NiO interacting with the support or NiAl<sub>2</sub>O<sub>4</sub> [55,59]. Formation of NiAl<sub>2</sub>O<sub>4</sub> was explained by Scheffer et al. [66]. Nickel ions diffused into the Al<sub>2</sub>O<sub>3</sub> support, where it was coordinated tetrahedrally and octahedrally to form NiAl<sub>2</sub>O<sub>4</sub>. UV of 5Ni3SiAl sample also detected Ni<sup>2+</sup> in tetrahedral and octahedral coordination. On the other hand, the H<sub>2</sub>-TPR profile of 5Ni3WAl catalyst was characterized by absence of region I peak (for free NiO)

and an additional peak in region IV [67]. The absence of free NiO species suggested that some interaction was occurred between NiO and  $\text{WO}_3$  or  $\text{Al}_2\text{O}_3$  species. Scheffer et al. discussed that from  $\text{NiAl}_2\text{O}_4$  species some of aluminium ions may be replaced and form new NiO species (or  $\text{NiWOAl}$ ) and the reduction peak of this new NiO species would be at higher temperature beside reduction peak of  $\text{NiAl}_2\text{O}_4$  species. Thus, additional peak in region IV can be claimed to reduction peaks of  $\text{NiWOAl}$  species. Further, the reduction peaks in regions II and III were largely overlapped in which region III was more prominent. Region II showed reduction peaks for  $\text{NiWO}_4$  species, whereas region III showed reduction peaks for  $\text{NiAl}_2\text{O}_4$  [56,60]. Overall, it can be said that  $5\text{Ni}_3\text{SiAl}$  catalyst system had  $\text{NiSiO}_3$  and  $\text{NiAl}_2\text{O}_4$  species, whereas  $5\text{Ni}_3\text{WAl}$  catalyst system had  $\text{NiWO}_4$  and  $\text{NiAl}_2\text{O}_4$  species majorly.

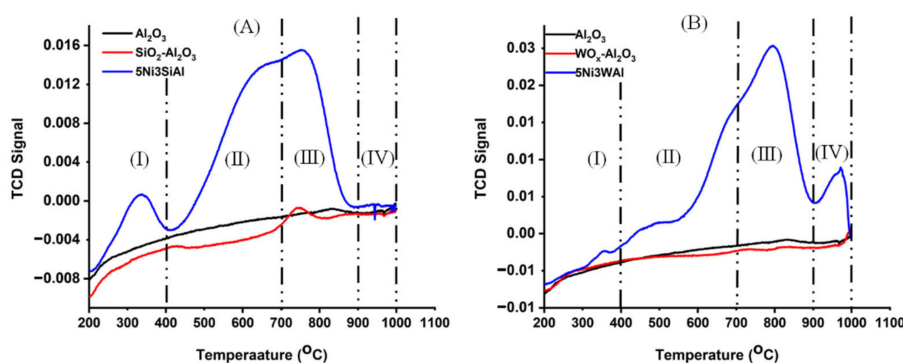


**Figure 6.**  $\text{H}_2$  temperature-programmed surface reduction profiles of (A)  $\text{Al}_2\text{O}_3$ , 3SiAl, and  $5\text{Ni}_3\text{SiAl}$  catalysts, and (B)  $\text{Al}_2\text{O}_3$ , 3WAl, and  $5\text{Ni}_3\text{WAl}$  catalysts.

### 3. Discussion

The chief route of  $\text{H}_2$  production via DRM comprises the dissociation of  $\text{CH}_4$  over the surface of Ni (or supported Ni) to produce carbon deposits and  $\text{H}_2$ , followed by the oxidation of the carbon deposits by  $\text{CO}_2$  to produce  $\text{CO}$  ( $\text{CH}_4 + \text{CO}_2 \rightarrow \text{CO} + \text{H}_2$ ). Nevertheless, the reverse water gas shift (RWGS) reaction due to a spill over effect of molecular hydrogen, produced over the surface of Ni, ( $\text{CO}_2 + \text{H}_2 \rightarrow \text{CO} + \text{H}_2\text{O}$ ) and the gasification of the carbon deposits by hydrogen gas ( $\text{C} + 2\text{H}_2 \rightarrow \text{CH}_4$ ) [68] are not reaction routes that can be ignored. In fact, these parallel reactions can affect  $\text{H}_2$  yield. Notably, not all parallel reactions, taking place over the catalyst surface, are detrimental to the mean yield of  $\text{H}_2$ . For instance, the presence of water at the catalyst surface (possibly due to RWGS) may contribute to the gasification of carbon deposits, leading to the production of molecular hydrogen and carbon monoxide ( $\text{C} + 2\text{H}_2\text{O} \rightarrow \text{CO} + \text{H}_2$ ), and thus increasing  $\text{H}_2$  yield.

The dispersion and stability of “Ni-related species” over a support determine the  $\text{H}_2$  yield of a DRM reaction, taking place over the surface of a catalyst. The  $5\text{Ni}_3\text{TiAl}$  catalyst was characterized by infrared-active Ni-O vibration frequencies close to those of free NiO; in fact, NiO interacted with the modifier to produce the characteristic peaks of  $\text{NiTiO}_3$ . UV-Vis absorption evidence also confirmed the presence of  $\text{Ni}^{2+}$  ions in an octahedral environment, in the form of segregated, crystallized, or bulk NiO, and the presence of  $\text{Ti}^{4+}$  in both tetrahedral and octahedral environments in  $\text{NiTiO}_3$ . Overall,  $5\text{Ni}_3\text{TiAl}$  comprised free NiO and  $\text{NiTiO}_3$ . XPS Al (2p) evidence on  $5\text{Ni}_3\text{TiAl}$  also confirmed the intact nature of  $\text{TiO}_2$  and NiO over the  $\text{Al}_2\text{O}_3$  support. The inferior catalytic performance of  $5\text{Ni}_3\text{TiAl}$  with respect to those of the other systems could be due to the free NiO species present in it. Use of  $5\text{Ni}_3\text{TiAl}$  as DRM catalyst was observed to be associated with a 30%  $\text{H}_2$  yield at 700 °C and more than 60% at 800 °C. The IR spectrum of  $5\text{Ni}_3\text{MoAl}$  did not include any peaks attributable to the vibration of the Ni-O bond of free NiO. The UV-Vis spectrum of  $5\text{Ni}_3\text{MoAl}$  was indicative of the presence of  $\text{Mo}^{6+}$  in octahedral/tetrahedral environments, as environment of  $\text{Mo}^{6+}$  in  $\text{NiMoO}_4$ . XPS Mo (3d) evidence on  $5\text{Ni}_3\text{MoAl}$

indicated the presence of a species, whereby NiO interacted with  $\text{MoO}_x$ , which was the dominant one, with a smaller prevalence of a species whereby NiO interacted with the support ( $\gamma\text{-Al}_2\text{O}_3$ ). The absence of free NiO in 5Ni3MoAl caused a larger fraction of Ni-interacted species with the modifier (as  $\text{NiMoO}_4$ ) at the surface than that at 5Ni3TiAl. An increased fraction of species whereby Ni interacted with  $\text{MoO}_x$  (i.e.,  $\text{NiMoO}_4$ ) caused the catalyst to increase in stability and resulted in >45%  $\text{H}_2$  yield of the DRM reaction at 700 °C. At high reaction temperature, about 800 °C, an endothermic feature of DRM reaction promoted enhanced  $\text{CH}_4$  decomposition at “Ni-interacted species surfaces” as  $\text{NiMoO}_4$  and  $\text{NiTiO}_3$  [69]. Therefore,  $\text{NiMoO}_4$  and  $\text{NiTiO}_3$  species (in 5Ni3MoAl and 5Ni3TiAl catalyst systems, respectively) displayed high catalytic efficiency and thermal stability at high temperatures, with an over 60%  $\text{H}_2$  yield of the DRM reaction at 800 °C.

The IR spectra of 5Ni3SiAl and 5Ni3WAl were characterized by vibrational frequencies due to a variety species, whereby NiO interacted with the modifier or the support. 5Ni3SiAl comprised species, whereby NiO interacted with the modifier to form  $\text{NiSiO}_3$  and with the support to produce  $\text{NiAl}_2\text{O}_4$ , much like 5Ni3WAl comprised species, whereby NiO interacted with the modifier to form  $\text{NiWO}_4$  and with the support to form  $\text{NiAl}_2\text{O}_4$ . UV-Vis absorbance data confirmed the presence of  $\text{Ni}^{2+}$  in tetrahedral and octahedral environments in  $\text{NiAl}_2\text{O}_4$  in both catalysts.  $\text{H}_2$ -TPR evidence validated the ability of these “interacting-Ni species” in both 5Ni3SiAl and 5Ni3WAl catalyst systems to undergo reduction. As both catalysts comprised a variety of stable interacting-NiO species, they displayed equally high catalytic efficiency. Use of both catalysts in the DRM reaction resulted in >60%  $\text{H}_2$  yield at 700 °C and >70%  $\text{H}_2$  yield at 800 °C over 420 min on stream. Evidence suggested that the  $\text{NiSiO}_3$ ,  $\text{NiWO}_4$ , and  $\text{NiAl}_2\text{O}_4$  mixed oxides present in 5Ni3SiAl and 5Ni3WAl were more thermally stable than the  $\text{NiTiO}_3$  and  $\text{NiMoO}_4$  mixed oxides present in 5Ni3TiAl and 5Ni3MoAl, respectively. The catalyst system, composed of 12.5 wt% Ni and 12.5 wt% Co and supported on  $\text{La}_2\text{O}_3$ , showed 31% and 60%  $\text{H}_2$  yield for the catalyst calcined at 700 °C and 900 °C, respectively [70]. The 5 wt% MgO-promoted Ni-Co/ $\text{Al}_2\text{O}_3$ -ZrO<sub>2</sub> nanocatalyst showed about 20%  $\text{H}_2$  yield at 650 °C and 40% hydrogen yield at 750 °C [71]. Ni catalysts supported on Gd-doped ceria (prepared by conventional impregnation method) showed 64%  $\text{H}_2$  yield [72]. The Sr-promoted  $\text{Al}_2\text{O}_3$  supported Nickel catalyst showed 70%  $\text{H}_2$  yield [73]. In our catalyst system, only 3 wt% promoter of either W or Si in  $\text{Al}_2\text{O}_3$ -supported nickel catalyst resulted into more than 60%  $\text{H}_2$  yield at 700 °C and more than 70%  $\text{H}_2$  yield at 800 °C. In the regeneration study with 5Ni3SiAl catalyst, the  $\text{H}_2$  yields after the first and second recycling were 58 and 59%, respectively at 700 °C. It can be inferred that the catalyst regained nearly all its performance after the removal of carbon deposits by using oxygen (Figure 7).

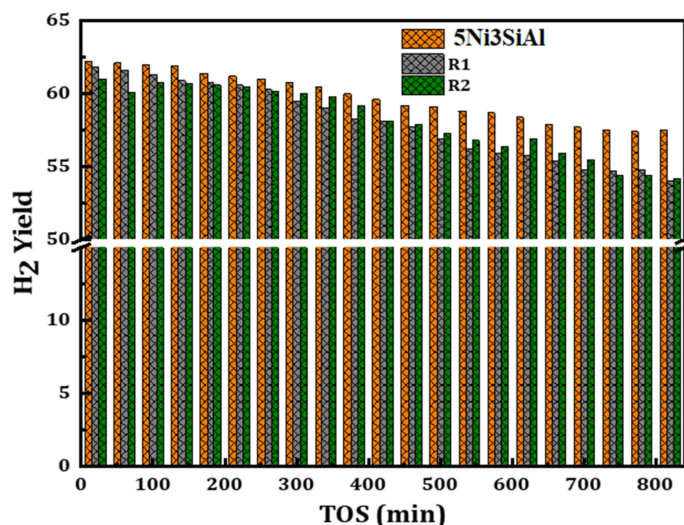


**Figure 7.**  $\text{H}_2$  yield over fresh 5Ni3SiAl catalyst,  $\text{H}_2$  yield after first cycle (R1), and  $\text{H}_2$  yield after second cycle (R2).

## 4. Materials and Methods

### 4.1. Catalyst Preparation

The 5Ni3MAI (M = Si, Ti, Mo, or W) catalyst systems were prepared by incipient wetness impregnation, followed by calcination. The detailed procedure for catalyst preparation is described as follows. The required amounts of well-grounded  $\gamma$ -Al<sub>2</sub>O<sub>3</sub> and metal oxides precursors ((NH<sub>4</sub>)<sub>6</sub>Mo<sub>7</sub>O<sub>24</sub>·4H<sub>2</sub>O (Sigma-Aldrich, St. Louis, MO, USA) or (NH<sub>4</sub>)<sub>10</sub>H<sub>2</sub>(W<sub>2</sub>O<sub>7</sub>)<sub>6</sub> (Aldrich)) were mixed together and then crushed mechanically by mortar and pestle. Droplets of deionized H<sub>2</sub>O was added to form a paste. The mechanical mixing was carried out until the dried compact mixture was accomplished. Wetting and drying processes of the solid mixture were done three times. The dried mixture was calcined in a programmable muffle furnace at 600 °C at the rate 3 °C/min for three hours.  $\gamma$ -Alumina with titania (3.0 wt% TiO<sub>2</sub>/ $\gamma$ -Al<sub>2</sub>O<sub>3</sub>) and silica (2.0 wt% SiO<sub>2</sub>/ $\gamma$ -Al<sub>2</sub>O<sub>3</sub>) in the form of pellets, were gifts from the Inorganic Chemistry Laboratory, Oxford University, Oxford, UK. Same as the above discussed procedure, the essential amount of Ni (NO<sub>3</sub>)<sub>2</sub>·6H<sub>2</sub>O along, with doped  $\gamma$ -Al<sub>2</sub>O<sub>3</sub> support were grounded, were made in paste form, and then were dried and calcined. The calcined 5 wt% NiO /3 wt% MO<sub>x</sub>- $\gamma$ -Al<sub>2</sub>O<sub>3</sub> (M = Ti, Mo, W, Si) catalysts were abbreviated as 5Ni3MAI (M = Ti, Mo, W, Si).

### 4.2. Catalyst Characterization

Catalysts were characterized by SEM, EDXS, IR, UV-Vis, and X-ray Photoelectron spectroscopy techniques and H<sub>2</sub>-TPR. The morphology of the catalyst samples was investigated by using a field emission scanning electron microscope (FE-SEM, model: JEOL JSM-7100 F, St. Lucia, Queensland, Australia), furnished with energy dispersive X-ray spectroscopy (EDXS) for surface elemental analysis. The Fourier transform infrared (FTIR) measurements were carried out by using IR Prestige-21 SHIMADZU, spectrophotometer, Kyoto, Japan. The spectra were documented in the range 400–4000 cm<sup>-1</sup> with 4 cm<sup>-1</sup> energy resolution, using KBr pellet. Ultraviolet-visible measurement was carried out by using V-570 JASCO, Eston, PA, USA) spectrophotometer. The spectra were registered in the range of 200–800 nm wavelength with resolution of 1 nm at a scanning speed of 200 nm/min. The XPS was carried out using Thermo Scientific X-ray Photoelectron Spectrometer, Manchester, UK. Monochromatic Al K $\alpha$  (1486.6 eV) radiation source operating at a power of 72 W with a pass energy of 50 eV for high resolution area scans and 200 eV for inspection scans was used. For charge adjustment, a one-point scale with the C1s peak moved to 285.0 eV was used. Temperature-programmed reduction (TPR) was carried out with the Micromeritics AutoChem II, Atlanta, GA, USA. 0.07 g of the sample (in sample holder) was degassed using argon at 150 °C for 60 min and then cooled to 25 °C. Further, it was heated to 800 °C at the rate of 10 °C/minute under 10% H<sub>2</sub> in argon flow. The flow rate of 10% H<sub>2</sub> in argon was set at 40 mL/minute. At the reactor outlet, thermal conductivity detector (TCD) monitors the gas mixture and peaks corresponding to the consumption of H<sub>2</sub> as a function of temperature were obtained.

### 4.3. Catalytic Reaction

The reaction was performed at atmospheric pressure in a tubular, stainless steel, fixed-bed micro-reactor (ID = 9 mm) (supplied by PID Eng and Tech, Madrid, Spain). 0.10 g catalyst was reduced under 20 mL/min flow of H<sub>2</sub> at 800 °C for 60 min. Now, nitrogen gas was passed through the reactor for 20 min to eliminate adsorbed H<sub>2</sub> at 700 °C. Afterwards, dry reforming of methane was carried out by passing CH<sub>4</sub>, CO<sub>2</sub>, and N<sub>2</sub> gas mixture feed at flow rates of 30, 30, and 10 mL/min respectively through the catalyst bed. The temperature, pressure and reaction variables were monitored through the reactor panel. GC-2014 (SHIMADZU, Kyoto, Japan) gas chromatograph equipped with Porapak Q and Molecular Sieve 5A columns and thermal conductivity detector was joined in series/bypass connections to have a whole examination of the reaction products and the feed. For regeneration process, fresh 5Ni-3SiO<sub>2</sub> + Al<sub>2</sub>O<sub>3</sub> catalyst is packed in the reactor. The sample was activated with H<sub>2</sub> flow of 20 mL/min for an hour and then followed by a

reaction for 820 min at 700 °C. The spent catalyst is then treated with 10 mL/min O<sub>2</sub> for 30 min to remove the deposited carbon. Subsequently, the recycled catalyst was activated with H<sub>2</sub> to take care of any oxidized Ni metal during the recycling and thereafter, reaction was performed. Again, the recycling operation was repeated and the reaction carried out the third time.

## 5. Conclusions

The titanium-modified catalyst (5Ni<sub>3</sub>TiAl) had free NiO and NiTiO<sub>3</sub> species. Free NiO species were completely unsuitable for H<sub>2</sub> production through DRM. The presence of the free NiO fraction caused 5Ni<sub>3</sub>TiAl to display about 30% H<sub>2</sub> yield at 700 °C. The molybdenum-modified catalyst (5Ni<sub>3</sub>MoAl) had no free NiO species, but had NiO interacting with MoO<sub>3</sub> species or NiMoO<sub>4</sub> species, which displayed a moderate catalytic performance of about 45% H<sub>2</sub> yield at 700 °C. Notably, at a higher reaction temperature (800 °C), the endothermic feature of the DRM reaction enhanced CH<sub>4</sub> decomposition, and both catalysts displayed a higher but equal efficiency of about 60% H<sub>2</sub> yield. On the other hand, the silicon-modified catalyst (5Ni<sub>3</sub>SiAl) and tungsten-modified catalyst (5Ni<sub>3</sub>WAl) were comprised of a variety of thermally stable species, whereby NiO interacted with the modifier and the support. The 5Ni<sub>3</sub>SiAl catalyst system had NiSiO<sub>3</sub> and NiAl<sub>2</sub>O<sub>4</sub> species, whereas the 5Ni<sub>3</sub>WAl catalyst system had NiWO<sub>4</sub> and NiAl<sub>2</sub>O<sub>4</sub> species. The sets of mixed oxides present in 5Ni<sub>3</sub>SiAl and 5Ni<sub>3</sub>WAl were responsible for displaying higher thermal stability and catalytic performance than 5Ni<sub>3</sub>TiAl and 5Ni<sub>3</sub>MoAl. In fact, the 5Ni<sub>3</sub>SiAl and 5Ni<sub>3</sub>WAl catalyst systems displayed equally high catalytic efficiency of about 60% H<sub>2</sub> yield at 700 °C and about 70% H<sub>2</sub> yield at 800 °C, over 420 min on stream. The 5Ni<sub>3</sub>SiAl catalyst regained nearly all its activity after the removal of carbon deposits by using oxygen.

**Supplementary Materials:** The following are available online at <https://www.mdpi.com/2227-9717/9/1/157/s1>, Figure S1: SEM image of different catalyst system; Figure S2: EDX spectra of different catalyst system, Figure S3: Infrared spectroscopy of different catalyst system, Figure S4: Deconvoluted H<sub>2</sub> temperature-programmed surface reduction profiles of (A) 5Ni<sub>3</sub>SiAl catalyst, and (B) 5Ni<sub>3</sub>WAl catalyst.

**Author Contributions:** A.S.A.-F., A.A.I., and S.O.K. synthesized the catalysts, carried out all the experiments and characterization tests, and wrote the manuscript. R.P., F.A.-M., and R.K. prepared the catalyst and contributed to proofreading of the manuscript. F.A.-M., M.L.C., Y.A.A., and A.A.B., writing—review and editing; A.H.F. contributed to the analysis of the data and proofread the manuscript. All authors have read and agreed to the published version of the manuscript.

**Funding:** The work is supported by the Deanship of Scientific Research programs of King Saud University via project No. RGP-119.

**Data Availability Statement:** Data is contained within the article.

**Acknowledgments:** The authors would like to express their sincere appreciation to the Deanship of Scientific Research at King Saud University for funding this research project (#RGP-119).

**Conflicts of Interest:** The authors declare no competing interests.

## References

1. Mazloomi, K.; Gomes, C. Hydrogen as an energy carrier: Prospects and challenges. *Renew. Sustain. Energy Rev.* **2012**, *16*, 3024–3033. [CrossRef]
2. Balat, M. Potential importance of hydrogen as a future solution to environmental and transportation problems. *Int. J. Hydrog. Energy* **2008**, *33*, 4013–4029. [CrossRef]
3. Ni, M.; Leung, D.Y.C.; Leung, M.K.H.; Sumathy, K. An overview of hydrogen production from biomass. *Fuel Process. Technol.* **2006**, *87*, 461–472. [CrossRef]
4. Wu, G.; Zhang, C.; Li, S.; Huang, Z.; Yan, S.; Wang, S.; Ma, X.; Gong, J. Sorption enhanced steam reforming of ethanol on Ni-CaO-Al<sub>2</sub>O<sub>3</sub> multifunctional catalysts derived from hydrotalcite-like compounds. *Energy Environ. Sci.* **2012**, *5*, 8942–8949. [CrossRef]
5. Clough, P.T.; Boot-Handford, M.E.; Zheng, L.; Zhang, Z.; Fennell, P.S. Hydrogen production by sorption enhanced steam reforming (SESR) of biomass in a fluidised-bed reactor using combined multifunctional particles. *Materials* **2018**, *11*, 859. [CrossRef]

6. Yu, D.; Aihara, M.; Antal, M.J. Hydrogen production by steam reforming glucose in supercritical water. *Energy Fuels* **1993**, *7*, 574–577. [[CrossRef](#)]
7. Schmieder, H.; Abeln, J.; Boukis, N.; Dinjus, E.; Kruse, A.; Kluth, M.; Petrich, G.; Sadri, E.; Schacht, M. Hydrothermal gasification of biomass and organic wastes. *J. Supercrit. Fluids* **2000**, *17*, 145–153. [[CrossRef](#)]
8. Osman, A.I.; Meudal, J.; Laffir, F.; Thompson, J.; Rooney, D. Enhanced catalytic activity of Ni on H-Al<sub>2</sub>O<sub>3</sub> and ZSM-5 on addition of ceria zirconia for the partial oxidation of methane. *Appl. Catal. B Environ.* **2017**, *212*, 68–79. [[CrossRef](#)]
9. Gutta, N.; Velisoju, V.K.; Tardio, J.; Patel, J.; Satyanarayana, L.; Sarma, A.V.S.; Akula, V. CH<sub>4</sub> Cracking over the Cu-Ni/Al-MCM-41 catalyst for the simultaneous production of H<sub>2</sub> and highly ordered graphitic carbon nanofibers. *Energy Fuels* **2019**, *33*, 12656–12665. [[CrossRef](#)]
10. Kumar, R.; Ponnada, S.; Enjamuri, N.; Pandey, J.K.; Chowdhury, B. Synthesis, characterization and correlation with the catalytic activity of efficient mesoporous niobia and mesoporous niobia-zirconia mixed oxide catalyst system. *Catal. Commun.* **2016**, *77*, 42–46. [[CrossRef](#)]
11. Tomiyama, S.; Takahashi, R.; Sato, S.; Sodesawa, T.; Yoshida, S. Preparation of Ni/SiO<sub>2</sub> catalyst with high thermal stability for CO<sub>2</sub>-reforming of CH<sub>4</sub>. *Appl. Catal. A Gen.* **2003**, *241*, 349–361. [[CrossRef](#)]
12. Al-Fatesh, A.S.A.; Ibrahim, A.A.; Fakeeha, A.H.; Abasaheed, A.E.; Siddiqui, M.R.H. Oxidative CO<sub>2</sub> reforming of CH<sub>4</sub> over Ni/ $\alpha$ -Al<sub>2</sub>O<sub>3</sub> catalyst. *J. Ind. Eng. Chem.* **2011**, *17*, 479–483. [[CrossRef](#)]
13. Kim, D.H.; Kim, S.Y.; Han, S.W.; Cho, Y.K.; Jeong, M.G.; Park, E.J.; Kim, Y.D. The catalytic stability of TiO<sub>2</sub>-shell/Ni-core catalysts for CO<sub>2</sub> reforming of CH<sub>4</sub>. *Appl. Catal. A Gen.* **2015**, *495*, 184–191. [[CrossRef](#)]
14. Seo, H.O.; Sim, J.K.; Kim, K.D.; Kim, Y.D.; Lim, D.C.; Kim, S.H. Carbon dioxide reforming of methane to synthesis gas over a TiO<sub>2</sub>-Ni inverse catalyst. *Appl. Catal. A Gen.* **2013**, *451*, 43–49. [[CrossRef](#)]
15. Shah, M.; Mondal, P.; Nayak, A.K.; Bordoloi, A. Advanced titania composites for efficient CO<sub>2</sub> reforming with methane: Statistical method vs. experiment. *J. CO<sub>2</sub> Util.* **2020**, *39*, 101160. [[CrossRef](#)]
16. Shah, M.; Bordoloi, A.; Nayak, A.K.; Mondal, P. Effect of Ti/Al ratio on the performance of Ni/TiO<sub>2</sub>-Al<sub>2</sub>O<sub>3</sub> catalyst for methane reforming with CO<sub>2</sub>. *Fuel Process. Technol.* **2019**, *192*, 21–35. [[CrossRef](#)]
17. Xu, Y.; Du, X.H.; Li, J.; Wang, P.; Zhu, J.; Ge, F.J.; Zhou, J.; Song, M.; Zhu, W.Y. A comparison of Al<sub>2</sub>O<sub>3</sub> and SiO<sub>2</sub> supported Ni-based catalysts in their performance for the dry reforming of methane. *Ranliao Huaxue Xuebao/J. Fuel Chem. Technol.* **2019**, *47*, 199–208. [[CrossRef](#)]
18. Zhou, L.; Li, L.; Wei, N.; Li, J.; Basset, J.-M. Effect of NiAl<sub>2</sub>O<sub>4</sub> formation on Ni/Al<sub>2</sub>O<sub>3</sub> stability during dry reforming of methane. *ChemCatChem* **2015**, *7*, 2508–2516. [[CrossRef](#)]
19. Shen, D.; Huo, M.; Li, L.; Lyu, S.; Wang, J.; Wang, X.; Zhang, Y.; Li, J. Effects of alumina morphology on dry reforming of methane over Ni/Al<sub>2</sub>O<sub>3</sub> catalysts. *Catal. Sci. Technol.* **2020**, *10*, 510–516. [[CrossRef](#)]
20. Fang, X.; Peng, C.; Peng, H.; Liu, W.; Xu, X.; Wang, X.; Li, C.; Zhou, W. Methane dry reforming over coke-resistant mesoporous Ni-Al<sub>2</sub>O<sub>3</sub> catalysts prepared by evaporation-induced self-assembly method. *ChemCatChem* **2015**, *7*, 3753–3762. [[CrossRef](#)]
21. Medeiros, R.L.B.A.; Figueredo, G.P.; Macedo, H.P.; Oliveira, Â.A.S.; Rabelo-Neto, R.C.; Melo, D.M.A.; Braga, R.M.; Melo, M.A.F. One-pot microwave-assisted combustion synthesis of Ni-Al<sub>2</sub>O<sub>3</sub> nanocatalysts for hydrogen production via dry reforming of methane. *Fuel* **2020**, 119511. [[CrossRef](#)]
22. Zhao, Y.; Kang, Y.; Li, H.; Li, H. CO<sub>2</sub> conversion to synthesis gas: Via DRM on the durable Al<sub>2</sub>O<sub>3</sub>/Ni/Al<sub>2</sub>O<sub>3</sub> sandwich catalyst with high activity and stability. *Green Chem.* **2018**, *20*, 2781–2787. [[CrossRef](#)]
23. Rahemi, N.; Haghghi, M.; Babaluo, A.A.; Jafari, M.F.; Khorram, S. Non-thermal plasma assisted synthesis and physicochemical characterizations of Co and Cu doped Ni/Al<sub>2</sub>O<sub>3</sub> nanocatalysts used for dry reforming of methane. *Int. J. Hydrog. Energy* **2013**, *38*, 16048–16061. [[CrossRef](#)]
24. Fakeeha, A.H.; Bagabas, A.A.; Lanre, M.S.; Osman, A.I.; Kasim, S.O.; Ibrahim, A.A.; Arasheed, R.; Alkhalifa, A.; Elnour, A.Y.; Abasaheed, A.E.; et al. Catalytic performance of metal oxides promoted nickel catalysts supported on mesoporous  $\gamma$ -Alumina in dry reforming of methane. *Processes* **2020**, *8*, 522. [[CrossRef](#)]
25. Yao, L.; Galvez, M.E.; Hu, C.; da Costa, P. Mo-promoted Ni/Al<sub>2</sub>O<sub>3</sub> catalyst for dry reforming of methane. *Int. J. Hydrog. Energy* **2017**, *42*, 23500–23507. [[CrossRef](#)]
26. Vroulias, D.; Gkoulemani, N.; Papadopoulou, C.; Matralis, H. W-modified Ni/Al<sub>2</sub>O<sub>3</sub> catalysts for the dry reforming of methane: Effect of W loading. *Catal. Today* **2020**, *355*, 704–715. [[CrossRef](#)]
27. Wei, Q.; Yang, G.; Yoneyama, Y.; Vitidsant, T.; Tsubaki, N. Designing a novel Ni-Al<sub>2</sub>O<sub>3</sub>-SiC catalyst with a stereo structure for the combined methane conversion process to effectively produce syngas. *Catal. Today* **2016**, *265*, 36–44. [[CrossRef](#)]
28. Al-Fatesh, A.S.; Naeem, M.A.; Fakeeha, A.H.; Abasaheed, A.E. CO<sub>2</sub> reforming of methane to produce syngas over  $\gamma$ -Al<sub>2</sub>O<sub>3</sub>-supported Ni-Sr catalysts. *Bull. Chem. Soc. Jpn.* **2013**, *86*, 742–748. [[CrossRef](#)]
29. Fouskas, A.; Kollia, M.; Kambolis, A.; Papadopoulou, C.; Matralis, H. Boron-modified Ni/Al<sub>2</sub>O<sub>3</sub> catalysts for reduced carbon deposition during dry reforming of methane. *Appl. Catal. A Gen.* **2014**, *474*, 125–134. [[CrossRef](#)]
30. Alipour, Z.; Rezaei, M.; Meshkani, F. Effects of support modifiers on the catalytic performance of Ni/Al<sub>2</sub>O<sub>3</sub> catalyst in CO<sub>2</sub> reforming of methane. *Fuel* **2014**, *129*, 197–203. [[CrossRef](#)]
31. Seok, S.H.; Sun, H.C.; Park, E.D.; Sung, H.H.; Jae, S.L. Mn-promoted Ni/Al<sub>2</sub>O<sub>3</sub> catalysts for stable carbon dioxide reforming of methane. *J. Catal.* **2002**, *209*, 6–15. [[CrossRef](#)]

32. Therdthianwong, S.; Siangchin, C.; Therdthianwong, A. Improvement of coke resistance of Ni/Al<sub>2</sub>O<sub>3</sub> catalyst in CH<sub>4</sub>/CO<sub>2</sub> reforming by ZrO<sub>2</sub> addition. *Fuel Process. Technol.* **2008**, *89*, 160–168. [[CrossRef](#)]
33. Laosiripojana, N.; Sutthisripok, W.; Assabumrungrat, S. Synthesis gas production from dry reforming of methane over CeO<sub>2</sub> doped Ni/Al<sub>2</sub>O<sub>3</sub>: Influence of the doping ceria on the resistance toward carbon formation. *Chem. Eng. J.* **2005**, *112*, 13–22. [[CrossRef](#)]
34. Chein, R.Y.; Fung, W.Y. Syngas production via dry reforming of methane over CeO<sub>2</sub> modified Ni/Al<sub>2</sub>O<sub>3</sub> catalysts. *Int. J. Hydrog. Energy* **2019**, *44*, 14303–14315. [[CrossRef](#)]
35. Li, K.; Pei, C.; Li, X.; Chen, S.; Zhang, X.; Liu, R.; Gong, J. Dry reforming of methane over La<sub>2</sub>O<sub>2</sub>CO<sub>3</sub>-modified Ni/Al<sub>2</sub>O<sub>3</sub> catalysts with moderate metal support interaction. *Appl. Catal. B Environ.* **2020**, *264*, 118448. [[CrossRef](#)]
36. Amin, M.H.; Mantri, K.; Newnham, J.; Tardio, J.; Bhargava, S.K. Highly stable ytterbium promoted Ni/γ-Al<sub>2</sub>O<sub>3</sub> catalysts for carbon dioxide reforming of methane. *Appl. Catal. B Environ.* **2012**, *119–120*, 217–226. [[CrossRef](#)]
37. Zhang, Y.; Zhang, S.; Zhang, X.; Qiu, J.; Yu, L.; Shi, C. Ni modified WC x catalysts for methane dry reforming. In *Advances in CO<sub>2</sub> Capture, Sequestration, and Conversion*; American Chemical Society: Washington, DC, USA, 2015; pp. 171–189.
38. Shi, C.; Zhang, S.; Li, X.; Zhang, A.; Shi, M.; Zhu, Y.; Qiu, J.; Au, C. Synergism in NiMoOx precursors essential for CH<sub>4</sub>/CO<sub>2</sub> dry reforming. *Catal. Today* **2014**, *233*, 46–52. [[CrossRef](#)]
39. Al-Fatesh, A.S.; Kumar, R.; Kasim, S.O.; Ibrahim, A.A.; Fakeeha, A.H.; Abasaeed, A.E.; Alrasheed, R.; Bagabas, A.; Chaudhary, M.L.; Frusteri, F.; et al. The effect of modifier identity on the performance of Ni-based catalyst supported on γ-Al<sub>2</sub>O<sub>3</sub> in dry reforming of methane. *Catal. Today* **2020**, *348*, 236–242. [[CrossRef](#)]
40. Vlaev, L.; Damyanov, D.; Mohamed, M.M. Infrared spectroscopy study of the nature and reactivity of a hydrate coverage on the surface of γ-Al<sub>2</sub>O<sub>3</sub>. *Colloids Surf.* **1989**, *36*, 427–437. [[CrossRef](#)]
41. Du, X.; Wang, Y.; Su, X.; Li, J. Influences of pH value on the microstructure and phase transformation of aluminum hydroxide. *Powder Technol.* **2009**, *192*, 40–46. [[CrossRef](#)]
42. Dyer, C.; Hendra, P.J.; Forsling, W.; Ranheimer, M. Surface hydration of aqueous γ-Al<sub>2</sub>O<sub>3</sub> studied by Fourier transform Raman and infrared spectroscopy-I. Initial results. *Spectrochim. Acta Part A Mol. Spectrosc.* **1993**, *49*, 691–705. [[CrossRef](#)]
43. El-Kemary, M.; Nagy, N.; El-Mehasseb, I. Nickel oxide nanoparticles: Synthesis and spectral studies of interactions with glucose. *Mater. Sci. Semicond. Process.* **2013**, *16*, 1747–1752. [[CrossRef](#)]
44. Zhou, G.; Soo Kang, Y. Synthesis and characterization of the nickel titanate NiTiO<sub>3</sub> Nanoparticles in CTAB Micelle. *J. Dispers. Sci. Technol.* **2006**, *27*, 727–730. [[CrossRef](#)]
45. Vijayalakshmi, R.; Rajendran, V. Effect of reaction temperature on size and optical properties of NiTiO<sub>3</sub> nanoparticles. *E-J. Chem.* **2012**, *9*, 282–288. [[CrossRef](#)]
46. Umopathy, V.; Neeraja, P.; Manikandan, A.; Ramu, P. Synthesis of NiMoO<sub>4</sub> nanoparticles by sol-gel method and their structural, morphological, optical, magnetic and photocatalytic properties. *Trans. Nonferrous Met. Soc. China* **2017**, *27*, 1785–1793. [[CrossRef](#)]
47. De Moura, A.P.; De Oliveira, L.H.; Rosa, I.L.V.; Xavier, C.S.; Lisboa-Filho, P.N.; Li, M.S.; La Porta, F.A.; Longo, E.; Varela, J.A. Structural, optical, and magnetic properties of NiMoO<sub>4</sub> nanorods prepared by microwave sintering. *Sci. World J.* **2015**, *2015*. [[CrossRef](#)]
48. Okuno, M.; Zotov, N.; Schmücker, M.; Schneider, H. Structure of SiO<sub>2</sub>-Al<sub>2</sub>O<sub>3</sub> glasses: Combined X-ray diffraction, IR and Raman studies. *J. Non-Cryst. Solids* **2005**, *351*, 1032–1038. [[CrossRef](#)]
49. Sadjadi, M.S.; Mozaffari, M.; Enhessari, M.; Zare, K. Effects of NiTiO<sub>3</sub> nanoparticles supported by mesoporous MCM-41 on photoreduction of methylene blue under UV and visible light irradiation. *Superlattices Microstruct.* **2010**, *47*, 685–694. [[CrossRef](#)]
50. Salleh, N.F.M.; Jalil, A.A.; Triwahyono, S.; Efendi, J.; Mukti, R.R.; Hameed, B.H. New insight into electrochemical-induced synthesis of NiAl<sub>2</sub>O<sub>4</sub>/Al<sub>2</sub>O<sub>3</sub>: Synergistic effect of surface hydroxyl groups and magnetism for enhanced adsorptivity of Pd (II). *Appl. Surf. Sci.* **2015**, *349*, 485–495. [[CrossRef](#)]
51. Mancheva, M.N.; Iordanova, R.S.; Klissurski, D.G.; Tyuliev, G.T.; Kunev, B.N. Direct mechanochemical synthesis of nanocrystalline NiWO<sub>4</sub>. *J. Phys. Chem. C* **2007**, *111*, 1101–1104. [[CrossRef](#)]
52. Torres-Mancera, P.; Ramírez, J.; Cuevas, R.; Gutiérrez-Alejandre, A.; Murrieta, F.; Luna, R. Hydrodesulfurization of 4,6-DMDBT on NiMo and CoMo catalysts supported on B<sub>2</sub>O<sub>3</sub>-Al<sub>2</sub>O<sub>3</sub>. *Catal. Today* **2005**, *107–108*, 551–558. [[CrossRef](#)]
53. Carraro, P.; Elías, V.; García Blanco, A.; Sapag, K.; Moreno, S.; Oliva, M.; Eimer, G. Synthesis and multi-technique characterization of nickel loaded MCM-41 as potential hydrogen-storage materials. *Microporous Mesoporous Mater.* **2014**, *191*, 103–111. [[CrossRef](#)]
54. Forzatti, P.; Mari, C.M.; Villa, P. Defect structure and transport properties of Cr<sub>2</sub>(MoO<sub>4</sub>)<sub>3</sub> and Al<sub>2</sub>(MoO<sub>4</sub>)<sub>3</sub>. *Mater. Res. Bull.* **1987**, *22*, 1593–1602. [[CrossRef](#)]
55. Strohmeier, B.R. Gamma-Alumina (γ-Al<sub>2</sub>O<sub>3</sub>) by XPS. *Surf. Sci. Spectra* **1994**, *3*, 135–140. [[CrossRef](#)]
56. Reddy, B.M.; Chowdhury, B.; Smirniotis, P.G. XPS study of the dispersion of MoO<sub>3</sub> on TiO<sub>2</sub>-ZrO<sub>2</sub>, TiO<sub>2</sub>-SiO<sub>2</sub>, TiO<sub>2</sub>-Al<sub>2</sub>O<sub>3</sub>, SiO<sub>2</sub>-ZrO<sub>2</sub>, and SiO<sub>2</sub>-TiO<sub>2</sub>-ZrO<sub>2</sub> mixed oxides. *Appl. Catal. A Gen.* **2001**, *211*, 19–30. [[CrossRef](#)]
57. Shok, J.; Raju, G.; Reddy, P.S.; Subrahmanyam, M.; Venugopal, A. Catalytic decomposition of CH<sub>4</sub> over NiO-Al<sub>2</sub>O<sub>3</sub>-SiO<sub>2</sub> catalysts: Influence of catalyst preparation conditions on the production of H<sub>2</sub>. *Int. J. Hydrog. Energy* **2008**. [[CrossRef](#)]
58. Kim, K.; Yang, S.; Baek, J.I.; Kim, J.W.; Ryu, J.; Ryu, C.K.; Ahn, D.G.; Shin, K. Distribution of NiO/Al<sub>2</sub>O<sub>3</sub>/NiAl<sub>2</sub>O<sub>4</sub> in the fabrication of spray-dry oxygen carrier particles for chemical-looping combustion. In *Advanced Materials Research*; Trans Tech Publications: Bach, Switzerland, 2011; Volume 311. [[CrossRef](#)]
59. Bianchi, C.L.; Cattania, M.G.; Villa, P. XPS characterization of Ni and Mo oxides before and after ‘in situ’ treatments. *Appl. Surf. Sci.* **1993**, *70–71*, 211–216. [[CrossRef](#)]

60. Anwar, M.; Hogarth, C.A.; Bulpett, R. Effect of substrate temperature and film thickness on the surface structure of some thin amorphous films of MoO<sub>3</sub> studied by X-ray photoelectron spectroscopy (ESCA). *J. Mater. Sci.* **1989**, *24*, 3087–3090. [[CrossRef](#)]
61. Nefedov, V.I.; Firsov, M.N.; Shaplygin, I.S. Electronic structures of MRhO<sub>2</sub>, MRh<sub>2</sub>O<sub>4</sub>, RhMO<sub>4</sub> and Rh<sub>2</sub>MO<sub>6</sub> on the basis of X-ray spectroscopy and ESCA data. *J. Electron Spectrosc. Relat. Phenom.* **1982**, *26*, 65–78. [[CrossRef](#)]
62. Zingg, D.S.; Makovsky, L.E.; Tischer, R.E.; Brown, F.R.; Hercules, D.M. A surface spectroscopic study of molybdenum-alumina catalysts using x-ray photoelectron, ion-scattering, and Raman spectroscopies. *J. Phys. Chem.* **1980**, *84*, 2898–2906. [[CrossRef](#)]
63. Schouten, F.C.; Kaleveld, E.W.; Bootsma, G.A. AES-LEED-ellipsometry study of the kinetics of the interaction of methane with Ni(110). *Surf. Sci.* **1977**, *63*, 460–474. [[CrossRef](#)]
64. Chen, Y.; Hu, C.; Gong, M.; Zhu, X.; Chen, Y.; Tian, A. Chemisorption of methane over Ni/Al<sub>2</sub>O<sub>3</sub> catalysts. *J. Mol. Catal. A Chem.* **2000**, *152*, 237–244. [[CrossRef](#)]
65. Guo, C.; Wu, Y.; Qin, H.; Zhang, J. CO methanation over ZrO<sub>2</sub>/Al<sub>2</sub>O<sub>3</sub> supported Ni catalysts: A comprehensive study. *Fuel Process. Technol.* **2014**, *124*, 61–69. [[CrossRef](#)]
66. Scheffer, B.; Molhoek, P.; Moulijn, J.A. Temperature-programmed reduction of NiO-WO<sub>3</sub>/Al<sub>2</sub>O<sub>3</sub> Hydrodesulphurization Catalysts. *Appl. Catal.* **1989**, *46*, 11–30. [[CrossRef](#)]
67. Southmayd, D.W.; Contescu, C.; Schwarz, J.A. Temperature-programmed reduction and oxidation of nickel supported on WO<sub>3</sub>-Al<sub>2</sub>O<sub>3</sub> composite oxides. *J. Chem. Soc. Faraday Trans.* **1993**, *89*, 2075–2083. [[CrossRef](#)]
68. Chung, U.C. Effect of H<sub>2</sub> on formation behavior of carbon nanotubes. *Bull. Korean Chem. Soc.* **2004**, *25*, 1521–1524. [[CrossRef](#)]
69. Al-Fatesh, A.S.; Kumar, R.; Fakeeha, A.H.; Kasim, S.O.; Khatri, J.; Ibrahim, A.A.; Arasheed, R.; Alabdulsalam, M.; Lanre, M.S.; Osman, A.I.; et al. Promotional effect of magnesium oxide for a stable nickel-based catalyst in dry reforming of methane. *Sci. Rep.* **2020**, *10*, 1–10. [[CrossRef](#)]
70. Fakeeha, A.H.; Khan, W.U.; Al-fatesh, A.S.; Ibrahim, A.A.; Abasaheed, A.E. Production of hydrogen from methane over lanthanum supported bimetallic catalysts. *Int. J. Hydrog. Energy* **2016**, *41*, 8193–8198. [[CrossRef](#)]
71. Sajjadi, S.M.; Haghighi, M.; Rahmani, F. Dry reforming of greenhouse gases CH<sub>4</sub>/CO<sub>2</sub> over MgO-promoted Ni-Co/Al<sub>2</sub>O<sub>3</sub>-ZrO<sub>2</sub> nanocatalyst: Effect of MgO addition via sol-gel method on catalytic properties and hydrogen yield. *J. Sol-Gel Sci. Technol.* **2014**, *70*, 111–124. [[CrossRef](#)]
72. Gurav, H.R.; Dama, S.; Samuel, V.; Chilukuri, S. Influence of preparation method on activity and stability of Ni catalysts supported on Gd doped ceria in dry reforming of methane. *J. CO<sub>2</sub> Util.* **2017**, *20*, 357–367. [[CrossRef](#)]
73. Ibrahim, A.A.; Fakeeha, A.H.; Al-Fatesh, A.S. Enhancing hydrogen production by dry reforming process with strontium promoter. *Int. J. Hydrog. Energy* **2014**, *39*, 1680–1687. [[CrossRef](#)]